The Pennsylvania State University

The Graduate School

MODELING AND SIMULATION OF THERMALLY MODULATED Li-ION BATTERIES FOR ELECTRIC AIRCRAFTS

A Thesis in

Mechanical Engineering

by

Shubham Suvarna

Submitted in Partial Fulfillment
of the Requirements
for the Degree of

Master of Science

May 2022

The thesis of Shubham Suvarna was reviewed and approved by the following:

Chao-Yang Wang
William E. Diefenderfer Chair of Mechanical Engineering
Thesis Advisor

Satadru Dey
Assistant Professor of Mechanical Engineering

Daniel Haworth
Professor of Mechanical Engineering
Chair of the Graduate Program

ABSTRACT

2021 was a remarkable year for widespread EV adoption and the advancement of Li-ion battery technology. Statistics show that EV sales were up 98% and are expected to grow at a similar pace in the future.[1] With an increase in demand for electrification, governments and companies around the world have allocated billions of dollars to produce energy dense Li-ion batteries. This development has opened a doorway for the future and the possibility of exploring the usage of Li-ion batteries in electric vertical takeoff and landing (EVTOL) aircrafts. Advancements in our ability to produce high energy density Li-ion has allowed us to impart a sufficient cruise range for EVTOL applications. However, conventional Li-ion batteries with high energy density do not always have sufficiently high power required for the takeoff and landing phases of travel. This thesis proposes using thermal modulation to increase the power density of an energy dense 100Ah Li-ion cell to meet the power requirements of EVTOL travel.

A 100 Ah Li-ion cell is modelled with thin nickel (Ni) foils embedded inside as internal heaters and simulation is conducted using a commercial software GT-Autolion. When current passes through the Ni foils, resistive heat is generated, and this heats up the cell from room temperature to 60°C. Heating the Li-ion cell provides an effective way to gain power on-demand from the battery. A switch sequence in the model enables the integration of heating effects from the Ni foil when required.

Exposing Li-ion batteries to high temperature for an elongated period of time can lead to severe degradation reactions within the battery. Accelerated growth of the solid electrolyte interface (SEI) layer can occur at high temperatures leading to irreversible loss of the capacity of the battery. Since the growth of the SEI layer is a function of time, we try and limit the cell's exposure to 60°C for a short period of time prior to takeoff and landing.

TABLE OF CONTENTS

LIST OF FIGURES

LIST OF TABLES

ACKNOWLEDGEMENTS

First, I would like to thank Dr. Chao-Yang Wang for his constant support, motivation and guidance through my research and graduate school at Penn State. I greatly appreciate your welcoming personality, mentorship and flexibility that has provided me with a well-rounded experience and helped me achieve my career goals. I am also grateful to Dr. Teng Lui and Dr. Shanhai Ge for their support on modelling and experimental data respectively.

I am extremely grateful to my mother Mohini Suvarna for providing me emotional, motivational, and financial support through my 6 years in college. Further, I would like to thank my grandmother (Gulabi Poojari), sister (Saakshi Suvarna) and father (Shashi Suvarna) for their prayers and encouragement that kept me going through all the difficult times. Lastly, I would like to take this opportunity to appreciate the contributions of two very important people in my life namely Tulasi Ram and Suhani Shah. Without your endless love, guidance and tolerance this masters' thesis would not have been complete.

Chapter 1

Introduction

1.1 Principles of Li-ion Batteries

Li-ion batteries mainly consists of a negative electrode (anode) and a positive electrode (cathode). Graphite due to its light weight and low electrode potential is the preferred anode material whereas high-rate capabilities make Li oxides the preferred cathode material. The anode and cathode are separated by a separator membrane that is impermeable to the flow of electrons but permeable to the flow of Li ions from one electrode to the other. The electrolyte provides a conductive pathway for the flow of Li ions. Lithium salts are the preferred electrolyte material due to their high ionic conductivity and low electrical conductivity.

Figure 1-1 depicts the negative graphite anode, a separator and the positive NMC cathode of an NMC-Graphite Li-ion battery. During discharge, the Li ions de-intercalate from the stored anode sites where they undergo the electrochemical reaction[2]

$$Li_xC_6 \rightarrow Li_0C_6 + xLi^+ + xe^- \quad (1.1)$$

and move to the cathode through the separator via diffusion and ionic conduction. At the NMC cathode the following electrochemical reaction takes place:[2]

$$Li_0NiMnCoO_2 + (1-x)Li^+ + (1-x)e^- \rightarrow Li_{(1-x)}NiMnCoO_2 \quad (1.2)$$

causing the positively charged ions to diffuse towards the solid phase of the metal oxide active material. The separator allows for the flow of ions but is impermeable to the flow of electrons, hence forcing the electrons through the external circuit. The end of the discharge cycle is characterized by an exponential drop in voltage and occurs when the Li concentrations in the

electrolyte phase becomes saturated. During the charging cycle the exact opposite processes and reactions take place transferring the Li ions back into the anode sites.

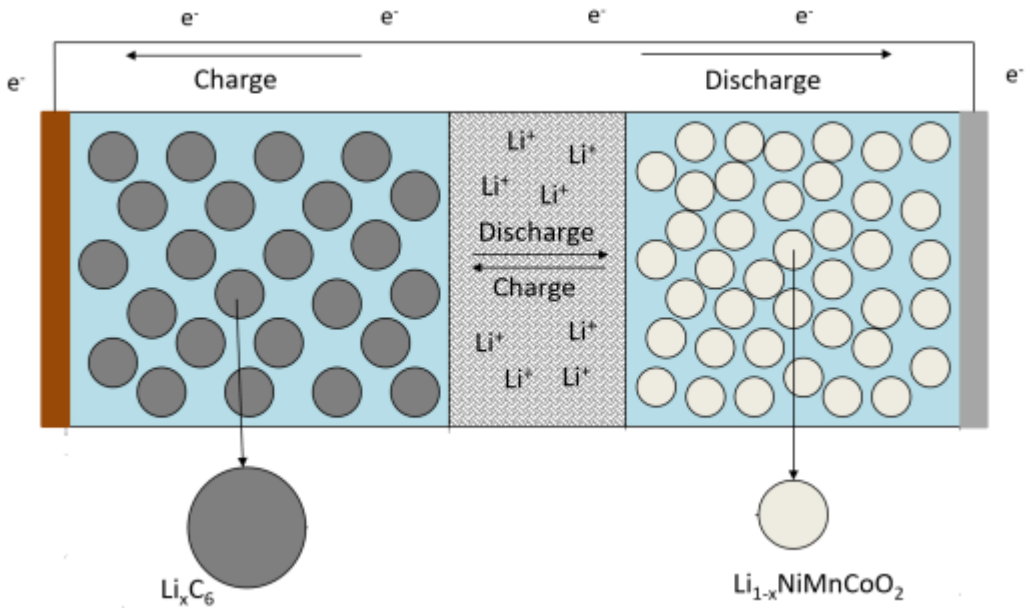

Figure **1-1**: A Pseudo-2D Model of NMC-Graphite Li-ion Battery (Su, Ke &Yuan, 2021, pp. 07)[3]

1.2 Electrochemical Modelling

Modelling of battery systems is often used to understand the behavior of cells in different conditions. Laboratory tests require expensive apparatus to control various experimental parameters and tests need to be run several times before desirable results are obtained. Hence, in such situations modelling provides us with a quick and cost-efficient way to analyze conditions and properties that could maximizes the performance of the battery. The physical properties of batteries are generally strong functions of temperature and state of charge (SOC). Electrochemical modelling is a useful tool to investigate how important battery parameter such as

direct current internal resistance (DCIR) and power density can vary with varying temperatures and SOC's.

There are three main electrochemical models that are used to simulate Li-ion battery systems. The pseudo two-dimensional model (P2D) was first proposed by Newman and Doyle in the 1900's.[4] The foundations of this model arise from charge conservation, material conservation, electrode reaction kinetics, ohm's law and the Li-ion diffusion in the electrolyte.[4] The input parameter in the P2D model have physical meaning and can effectively describe both the internal and external characteristics of the Li-ion battery at the same time.[5] The P2D model is used in this study via GT-Autolion.

The single particle model (SP) was first proposed by B S Haran.[5] The SP model assumes that the electric potential of the solid phase is equal everywhere in the electrode and the concentration of lithium ions in the liquid phase are equal everywhere in the battery.[5,6] As compared to the P2D model, the SP model introduces assumptions that lead to fewer equations and parameters which in turn simplifies the calculation process of the model.[5] Due to the assumption made, the SP model is only used for low charge rate and discharge calculations.[5,7]

Several scholars have proposed changes to the SP model to create an extended SP model depending on their areas of interest. For example, Luo W and Lyu C introduced the liquid phase diffusion process and the effect of heterogenous reaction distribution into the SP model to propose an extended SP model that could charge and discharge at 4C.[5,8] Whereas, Goto and Ohkuma inculcated concentration distribution of lithium electrolyte into the SP model to form their version of the extended SP model.[5,9]

Due to the continuous progress of electrochemical modelling technology through the years, there now lies an opportunity to employ these models and increase our understanding of cell behaviors in different environmental conditions.

1.3 Research Contributions

1.3.1 Research Motivation

With modern urbanization and the growing populations in cities, there arises a need to resolve traffic congestion by providing a quicker, more convenient and energy efficient mode of transport.[10] Electric vertical takeoff and landing (EVTOL) aircraft technology has emerged as a promising candidate to transform the future of transportation. EVTOL aircraft have electric powertrains that provide low noise and environmental impact.[10] Further, they combine a helicopters convenience of local takeoff and landing with an airplane's efficient aerodynamics.[10] Compared to the usage of Li-ion batteries in current industrial applications, EVTOL's have unique operating profiles and hence have drastically different power and energy requirements for different phases of the trip[10]. More specifically, high peak power is required during the takeoff and landing phases of the EVTOL trip whereas lower average power is sufficient during the cruise phase.

It is also likely that approval of a commercial EVTOL would require the aircraft to comply with stringent safety requirements. For example, the cell-to-cell propagation of thermal runway must be prevented in EVTOL batteries, and the aircraft must be able to continue flying on reduced power to allow for an emergency landing.[10] Further, building a fast-charging network is required to support peak travel requirements in urban areas and is paramount to the widespread acceptance and usage of EVTOL aircrafts.[10]

In order to accelerate our transition to sustainable sources of energy and resolve traffic congestion in densely populated metropolitan areas it is essential that we make progress in battery technology to satisfy the requirements for EVTOL.

1.3.2 Overview of the Present Work

This thesis will explore the power density requirements for EVTOL aircrafts during different phase of travel both numerically and through simulation.

Chapter 2 provides a detailed explanation of the electrochemical and thermal characteristics of the model. The controlling design and experimental parameters are described alongside the experimental setup for charge and discharge tests. Lastly, experimental validation of an 100Ah NMC811-Gr Li-ion cell is conducted at different temperatures.

Chapter 3 describes the creation of the thermally modulated model that uses a Ni-foil to heat and increase the battery temperature when required. This chapter starts with an analysis of how temperature and SOC affects important battery parameters. Numerical calculations are conducted to find the power density requirements in different phases of EVTOL travel. A GT-suite model is then constructed, and the power load profile is subjected to the model. Further, analysis of the power and energy density is conducted for different cruise periods and heating effects.

Chapter 4 provides a summary of the findings presented in this thesis. Further, this section also discusses some safety considerations that must be analyzed before the battery could be used in commercial applications.

Chapter 2

Model Development and Validation

In this thesis we explore the use of an 100Ah prismatic Li-ion battery for EVTOL applications. The prismatic Li-ion battery consist of five layers namely: the positive current collector (Al foil), the cathode (NMC 811), separator, the anode (graphite) and the negative current collector (Cu foil). These layers are stacked upon one another as shown in Figure 2-1 and enclosed in the cell can. A CAD model is created in Figure 2-2 to depict the external prismatic battery casing.

The electrolyte is present in the porous spaces within the separator, anode and cathode and provides a medium for Li-ion transport during charging and discharging. The Al and Cu foil, by virtue of their high electrical conductivity, facilitate the flow of electrons through the external circuit. This study employs a 1D model, wherein the current and ion transport occurs mainly in the thickness direction of anode, cathode and the separator. Further, experimental results are used to validate and calibrate the 1D model before any simulations are performed.

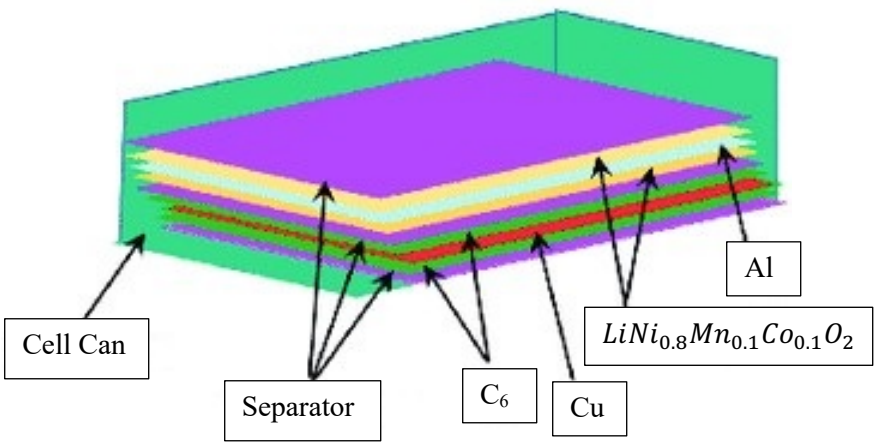

Figure **2-1**: Depiction of the Layers within a Prismatic Li-ion Battery (Dong Li, 2019, pp. 09)[19]

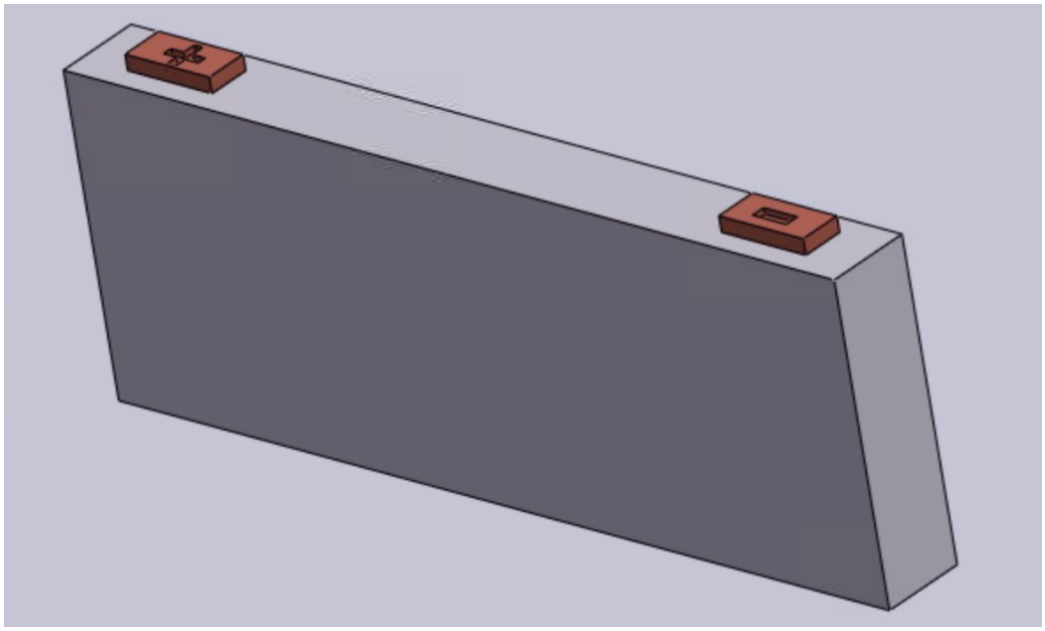

Figure **2-2**: CAD model of a Prismatic Li-ion Battery Design

2.1 Electrochemical Thermal Coupled (ECT) Model

2.1.1 Pseudo-2D Approach

The electrochemical modelling in this study uses the porous electrode theory combined with the concentrated solution theory as proposed by Neuman.[4] The 1D electrochemical processes take place through the porous electrodes with Li diffusion in spherical particles forming the Pseudo-2D approach.[12] The coupling between the electrochemical and thermal properties are accounted for by the internal heat generated, external heat transfer and the strong dependency of the material's kinetic and transport property on temperature.[13] Internal heaters in the form of Ni-foils are present within the battery model and are capable of heating the battery to extract power

on-demand. GT-Autolion, a commercial software, is used in this study to solve the following equations for battery simulation. The equations are obtained from our previous studies.[12,13]

Charge conservation in solid phase:

This describes the potential drop caused by the ohmic resistance in the electrodes

$$\frac{dI_s}{dx} = \frac{d}{dx}\left(-\sigma_s{}^{eff}\frac{d\varphi_s}{dx}\right) = -j \tag{2.1}$$

where φ_s is the electric potential of solid phase, $\sigma_s{}^{eff}$ is the effective electric conductivity of the solid electrode and j is the reaction current per unit volume.

Change conservation in electrolyte:

This describes the concentration overpotential in combination with the potential drop caused by the ohmic resistance in the electrolyte

$$\frac{dI_e}{dx} = \frac{d}{dx}\left(-\kappa^{eff}\frac{d\varphi_e}{dx} - \kappa_D^{eff}\frac{d\ln c_e}{dx}\right) = -j \tag{2.2}$$

where κ^{eff} is the effective ionic conductivity of the electrolyte, φ_e is the electric potential of the electrolyte and c_e is the electrolyte concentration.

Further, κ_D^{eff} is the effective diffusional ionic conductivity and is calculated as

$$\kappa_D^{eff} = \frac{2RT\kappa^{eff}}{F}(t_+^0 - 1)(1 + \frac{d\ln f_+}{dlnc_e}) \tag{2.3}$$

where R is the universal gas constant, T is the temperature, F is the faraday constant, t^+ is the li ion transfer number and $\frac{d\ln f_+}{dlnc_e}$ gives us the short-range ion-solvent interactions which become relevant for high concentration solutions.

Additionally, the volumetric current density in the charge conservation equations can be calculated as

$$j = \frac{3(1-\varepsilon)}{r_i}i \tag{2.4}$$

where ε is the porosity, r_i is the particle radius and i is the reaction current density.

Species conservation in electrolyte:

This describes the distribution of the electrolyte concentration and the surface kinetics governed by a diffusion process

$$\frac{d(\varepsilon c_e)}{dx} = \frac{d}{dx}\left(-D_e^{eff}\frac{dc_e}{dx}\right) + \left(\frac{1-t_+^0}{F}\right)j \tag{2.5}$$

where D_e^{eff} is the effective salt diffusivity modelled Bruggeman relation $D_e^{eff} = \mathrm{D_e}\,\varepsilon^p$

Species conservation in the active material (Fick's Law):

This describes the equilibrium potential and the lithium stoichiometry in solid particles

$$\frac{dc_s}{dt} = \frac{1}{r^2}\frac{d}{dr}\left(\mathrm{r}^2 D_s\frac{dc_s}{dr}\right), -D_s\left[\frac{dc_s}{dr}\right]_{r=R_0} = \frac{i}{F} \tag{2.6}$$

Where c_s is the lithium concentration in solid particles, D_s is lithium solid diffusivity and I is the local current density on particle surface.

Butler-Volmer equation:

This equation describes the kinetics of lithium insertion/deintercalation at the active material/electrolyte interface

$$i = i_0\left[\exp\left(\frac{\alpha_a F}{RT}\eta\right) - \exp\left(-\frac{\alpha_c F}{RT}\eta\right)\right] \tag{2.7}$$

where α_a and α_c are transfer coefficient of the anodic and cathodic reactions. The value of i_0 can be calculated by

$$i_0 = k c_{s,i}^{\alpha_c} c_e^{\alpha_a}(c_{s,max} - c_{s,i})^{\propto a} \tag{2.8}$$

where k is the reaction rate constant.

Further, surface overpotential is the potential difference between the solid and electrolyte phase at the reaction interface and is described as

$$\eta = \varphi_s - \varphi_e - U - iR_f \tag{2.9}$$

where U is the equilibrium potential and R_f is the particle surface film resistance.

Arrhenius Equation:

This equation describes the thermal dependence of the electrochemical properties

$$\Psi(T) = \Psi_{ref} \exp\left(\frac{E_{act}}{R}\left(\frac{1}{T_{ref}} - \frac{1}{T}\right)\right) \quad (2.10)$$

To account for tortuosity the effective parameters in a porous medium are expressed as a function of porosity and Bruggeman exponents

$$\Psi_s^{eff} = (1-\varepsilon)^p \Psi_s \; and \; \Psi_e^{eff} = \varepsilon^p \Psi_e \quad (2.11)$$

Heat generation:

This includes the heat generation at the reaction surface ($\dot{q}_i$), heat generation through the electrolyte ($\dot{q}_e$), ohmic heat generation through the solid electrodes ($\dot{q}_s$) and reversible heat ($\dot{q}_{rev}$).

$$\dot{Q}_{gen} = A_E \int_0^L (\dot{q}_i + \dot{q}_e + \dot{q}_s + \dot{q}_{rev}) dx \quad (2.12)$$

where A_E is the electrode area and L is the sum of the anode, cathode and separator thicknesses

$$\dot{q}_i = j(\varphi_s - \varphi_e - U) \quad (2.13)$$

$$\dot{q}_e = I_e\left(-\frac{d\varphi_e}{dx}\right) = \kappa^{eff}\left(\frac{d\varphi_e}{dx}\right)^2 + \kappa_D^{eff}\frac{d\varphi_e}{dx}\frac{dln(c_e)}{dx} \quad (2.14)$$

where I_e is the electrolyte current

$$\dot{q}_s = I_e\left(-\frac{d\varphi_s}{dx}\right) = \left(\frac{d\varphi_s}{dx}\right)^2 \sigma_s^{eff} \quad (2.15)$$

$$\dot{q}_{rev} = j\left(T\frac{dU}{dT}\right) \quad (2.16)$$

Energy conversation of the whole cell:

This equation determines the evolution of battery temperature in the form of a lumped model

$$mc_p\frac{dU}{dT} = \dot{Q}_{gen} - h(T - T_\infty)A_s \quad (2.17)$$

where c_p is the specific heat capacity, h is the convective heat transfer coefficient, A_s is the cell surface area and T_∞ is the temperature of the surrounding.

These equations form a series of nonlinear partial differential equation that are discretized and solved using GT-Autolion.[20]

2.1.2 Model Parameters and Design Parameters

The electrochemical and geometric parameters of the model were used in accordance with the design parameters of an energy dense Li-ion cell (100Ah) manufactured in our lab. Table 1 shows some important design characteristics of the cell. The heat transfer coefficient was determined by monitoring the cell temperature variation of the prismatic battery model at low C rates. The constants within the model were used as per industry standards, fitted from experiments and after extensive literature surveys on NMC-Graphite Li-ion cells.[10] Table 2 represents some important model parameters used in GT-Autolion.

Table **1** – Design parameters of the Li-ion cell

Parameters	**Anode**	**Separator**	**Cathode**
	Graphite (Gr)	**Celgard-2325**	$\boldsymbol{LiNi_{0.8}Mn_{0.1}Co_{0.1}O_2}$
Specific capacity, $\frac{mAh}{g}$	350	-	193
Porosity, ε	0.3	-	0.3
Capacity of active material, $\frac{Ah}{g}$	0.350	-	0.193
Weight fraction of the active materials, %	97.7	-	97.7

Specific energy of cell (4 Ah test cell), $\frac{Wh}{kg}$	237
Specific energy of cell (100 Ah cell), $\frac{Wh}{kg}$	231.7
Electrolyte composition	1M LiPF6 in EC/EMC

Table **2** – Model parameters of the Li-ion cell[10]

Properties	**Graphite (Gr)**	**Separator**	$\boldsymbol{LiNi_{0.8}Mn_{0.1}Co_{0.1}O_2}$
Solid-state diffusivity, $\frac{cm^2}{s}$	$2e^{-10}(1.5\text{-}x)^{1.5}$	-	$2e^{-10}(1.5\text{-}x)^{1.5}$
Activation energy of solid-state diffusivity, $\frac{kJ}{mol}$	65	-	65
Exchange current density, $\frac{mA}{cm^2}$	$0.21[2x^{0.5}c_e^{0.5}(1\text{-}x)^{0.5}]$	-	$0.21[2x^{0.5}c_e^{0.5}(1\text{-}x)^{0.5}]$
Activation energy of exchange current density, $\frac{kJ}{mol}$	65	-	65
Particle radius, μm	10	-	3
Charge transfer coefficient, α_a, α_c	0.5,0.5	-	0.5,0.5
Film resistance, Ωcm^2	0	-	0
Bruggeman factor	2.2	2	2.1
Specific heat of the cell, $\frac{J}{kgK}$	1200	-	-

2.2 Model Validation

2.2.1 Experimental Setup

To validate the electrochemical model, experimental 4-Ah pouch cells were set up and subjected to rate performance tests at different temperatures in our lab. These cells use the same electrodes and electrolyte as the model but for convenience and material usage were smaller in size.[22] All results from the 4-Ah pouch cells can be extrapolated to the 100-Ah prismatic design.[21] A standard constant current constant voltage (CCCV) procedure is used to charge the cell initially in the lab.[22] Further, discharge tests at different C rates are conducted and the voltage and temperature monitored during the discharge.[22] Tests are performed at room temperature (20°C), low temperature (10°C, 0°C) and high temperature (60°C) ranges in order to validate the model for all operating temperatures. A higher cutoff voltage of 4.2V and a lower cutoff voltage of 2.7V is used for the process. The experimental results from the 4-Ah cell are adjusted for validation of the 100-Ah prismatic model by comparing the cathode areas and the heat transfer characteristics of the shape. The cathode area of the 100-Ah prismatic model was found to be about 23 times larger than that of the 4-Ah experimental pouch cell and hence all experimental capacity readings of the pouch cell were multiplied by a factor of 22.73. It was found through simulation calibration that translating the same electrodes from pouch cell to prismatic cell required 4 times increase in the heat transfer coefficient to account for the thickness average heat generation in the 1D analysis. Therefore, the GT-Autolion model was set to a heat transfer coefficient of 80 $\frac{W}{Km^2}$ for validation purposes.

2.2.2 Validation Curves

To ensure that our model predictions remained consistent with experimental data, the model was validated for the charge and discharge tests conducted in our lab. The present work compares voltage and temperature curves at different charge rates and thermal environments. As mentioned earlier, the capacity readings are modified by a factor of 22.73 to account for the size and geometrical difference between the 4Ah pouch test cell and the 100Ah prismatic model.

Figures 2-3 and 2-4 depicts cells discharged at various charge rates starting at room temperature (20°C). Both the voltage and temperature as a function of discharge capacity show excellent agreement between model prediction and experimental data. As expected, the cell temperature increases faster when the cell is discharged at a higher C rate due to the larger amount of heat generation from the voltage losses.

Figure 2-5, 2-6, 2-7 and 2-8 depicts cells discharged at various C rates starting at temperatures below the room temperature. It can be observed that the capacity is significantly lowered, and the temperature rise is more prevalent due to large voltage losses and higher internal resistance in low temperature operations. The model predictions match well at low C rates, however when discharged at high C rates, the model underpredicts on voltages near the cutoff voltage. This can be attributed to the high sensitivity of the cell performance on operation conditions, design parameters and material properties at low temperatures.[14]

Figure 2-9 depicts cells charged at high charge rates and at a constant temperature of 20°C. It can be seen that the experimental and model results match well when voltage is plotted as a function of capacity. This can be attributed to increased kinetics and mass transport at high temperatures.[14]

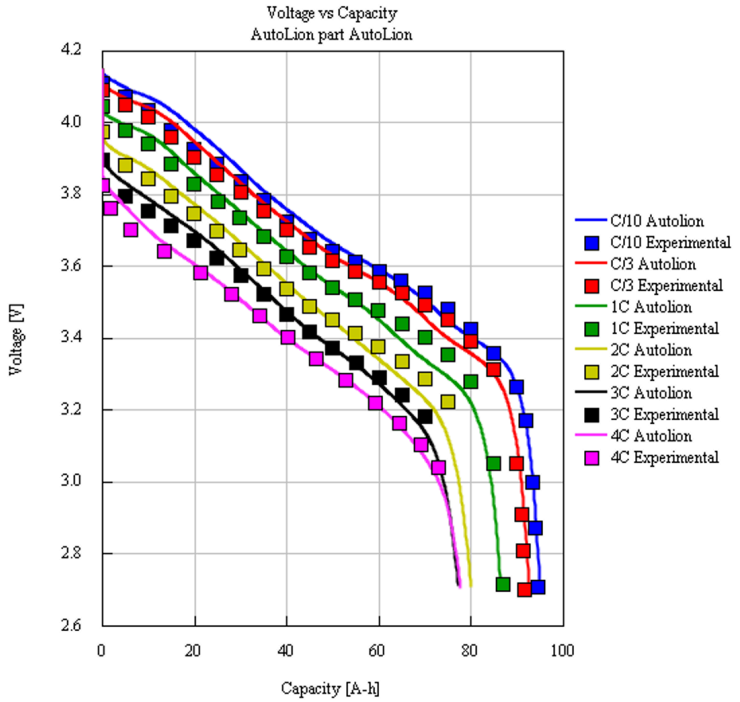

Figure **2-3**: Room Temperature (20°C) Validation- Voltage Discharge Curves

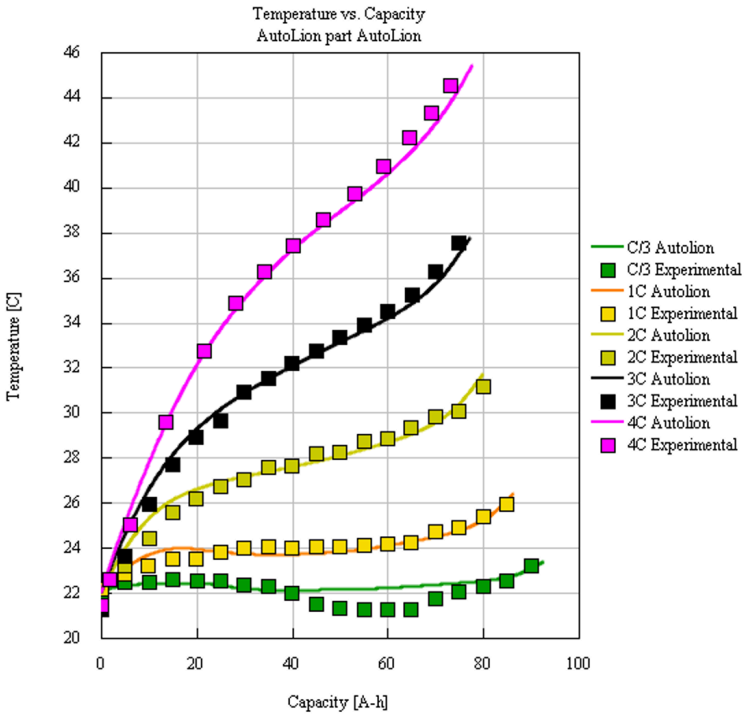

Figure **2-4**: Room Temperature (20°C) Validation- Temperature Curve

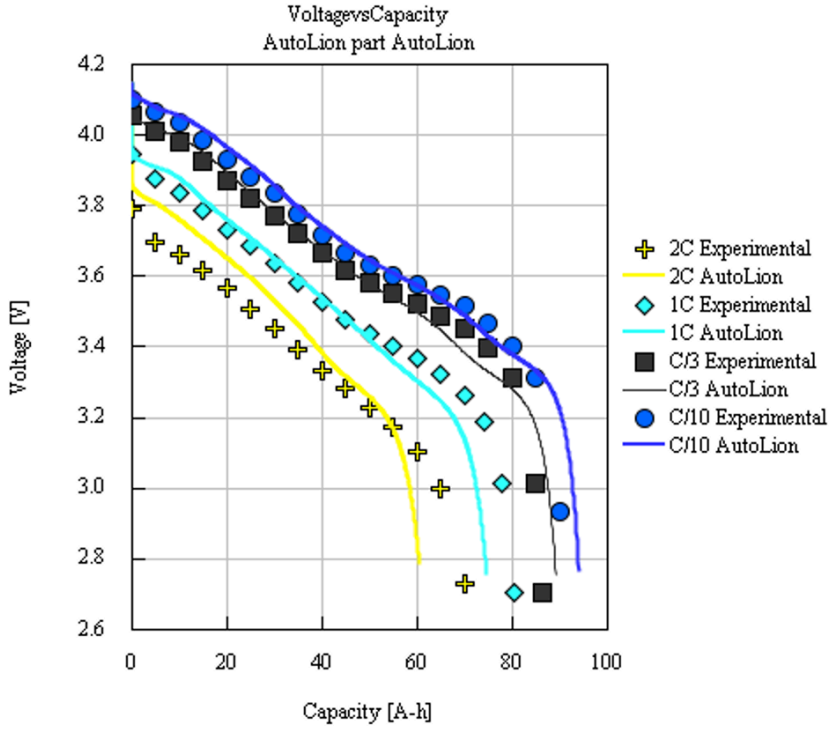

Figure **2-5**: Low Temperature (10°C) Validation- Voltage Discharge Curve

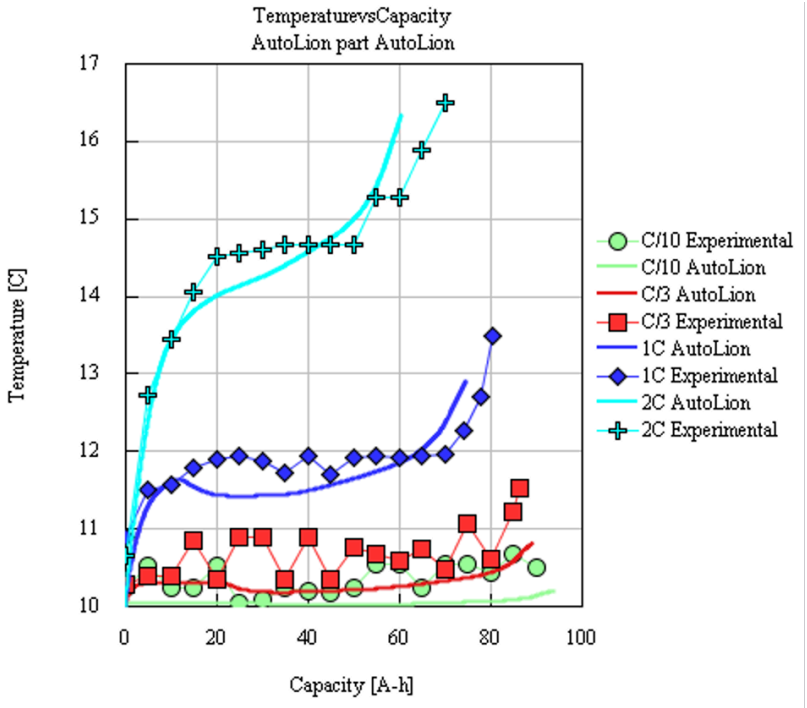

Figure **2-6**: Low Temperature (10°C) Validation- Temperature Curve

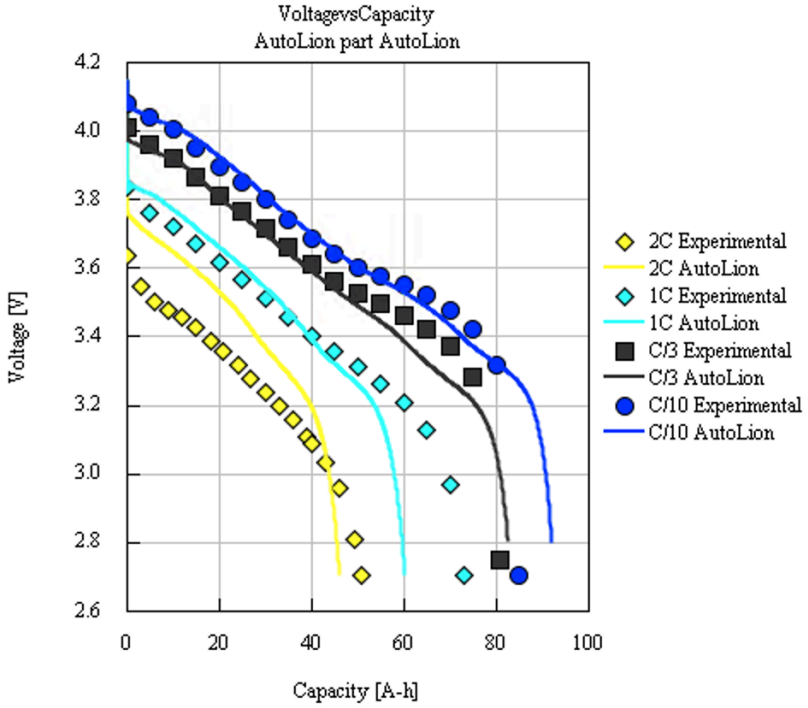

Figure **2-7**: Low Temperature (0°C) Validation- Voltage Discharge Curve

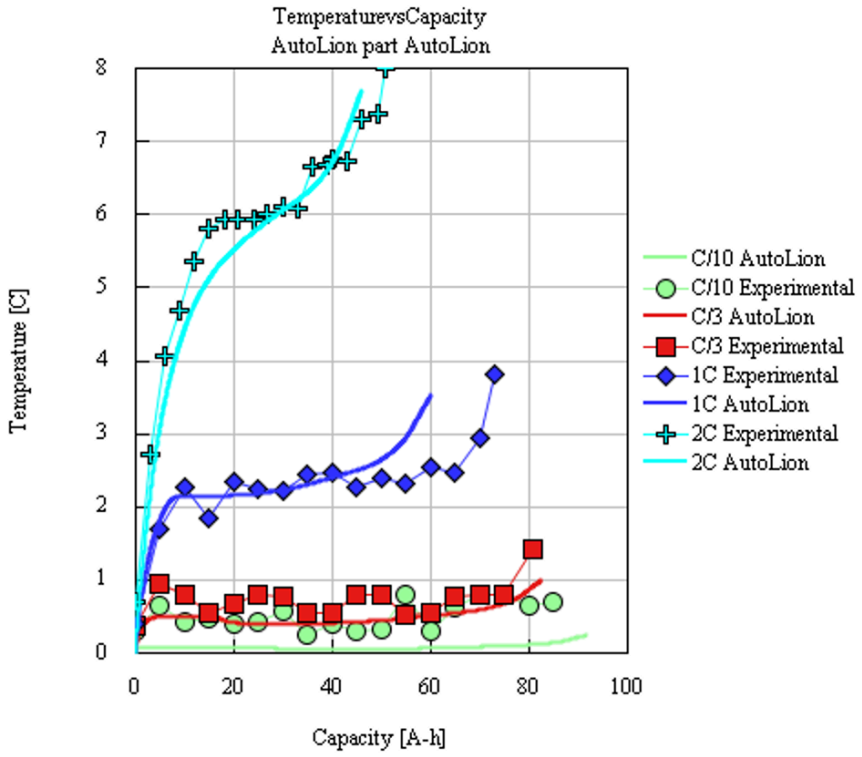

Figure **2-8**: Low Temperature (0°C) Validation- Temperature Curve

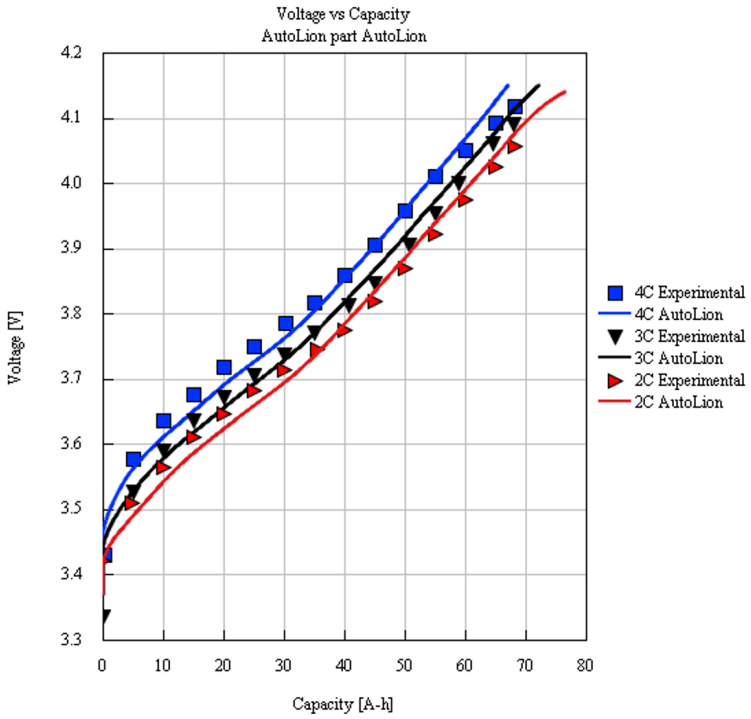

Figure **2-9**: High Temperature (60°C) Validation- Voltage Charge Curve

Chapter 3

Thermal Modulation for EVTOL Aircraft Applications

This chapter discusses the possibility of taking advantage of the high sensitivity of battery properties on temperature. Presented is a thermally modulated NMC-Graphite battery that is modelled to internally heat and operate at an elevated temperature of around 60°C when high power density is a requirement. Operating at a higher temperature boosts the kinetic and transport properties, giving rise to fast charging and remarkable power in all climates.[15] This is a cheaper and safer alternative than using large energy dense batteries which results in an increase in the gross weight of the aircraft and adds to its size. This concept has tremendous potential and the opportunity to bring large scale EVTOL adoption into the transportation sector.

3.1 Direct Current Internal Resistance (DCIR)

EVTOL applications require batteries to have high-energy and high-power density. However, energy is of limited use if the battery cannot deliver this energy efficiently. Direct current internal resistance (DCIR) dictates the ease in which stored energy is released from the cell. High internal resistances cause heating of the cell and sudden voltage drops which results in unnecessary losses of the stored energy. With lower DCIR, the cell experiences less restrictions during the discharge cycle. DCIR is extremely sensitive to temperature and SOC at which the battery operates. To calculate the DCIR, a user-defined step function is created with a 200A (charging) pulse current and a -150A (discharging) pulse current. The charging and discharging current are incident upon the model for 10 seconds each with a 50 seconds rest period between the two. Voltage data from the simulation is analyzed to calculate the DCIR values using the following equation:

$$DCIR = \frac{V_{afterpulse} - V_{beforepulse}}{I_{afterpulse} - I_{beforepulse}} \quad (3.1)$$

The process is repeated at different temperatures and SOCs and results plotted in figure 3-1 and 3-2 respectively. As temperature decrease the DCIR increases exponentially and reaches very high values at freezing temperatures. This could be attributed to slower chemical kinetics at lower temperatures. DCIR seems to be remain about constant with higher values of SOCs but increase significantly as we approach values below 10% SOC. It is therefore advisable that we always have reserve power while operating an EVTOL.

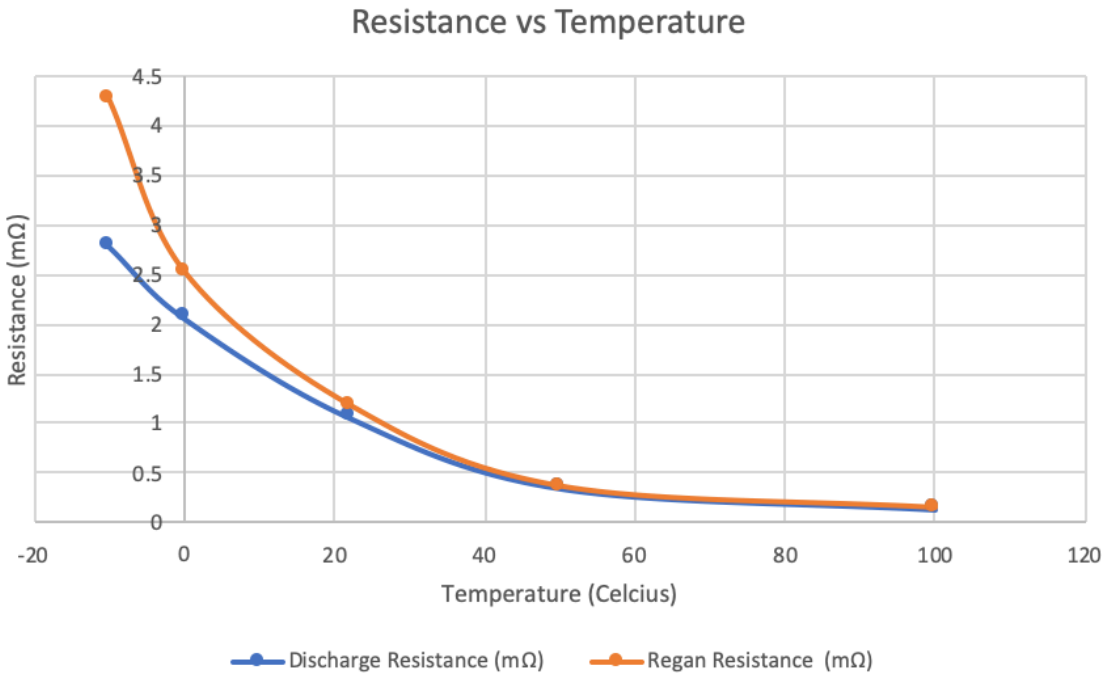

Figure **3-1**: Variation of DCIR with Temperature

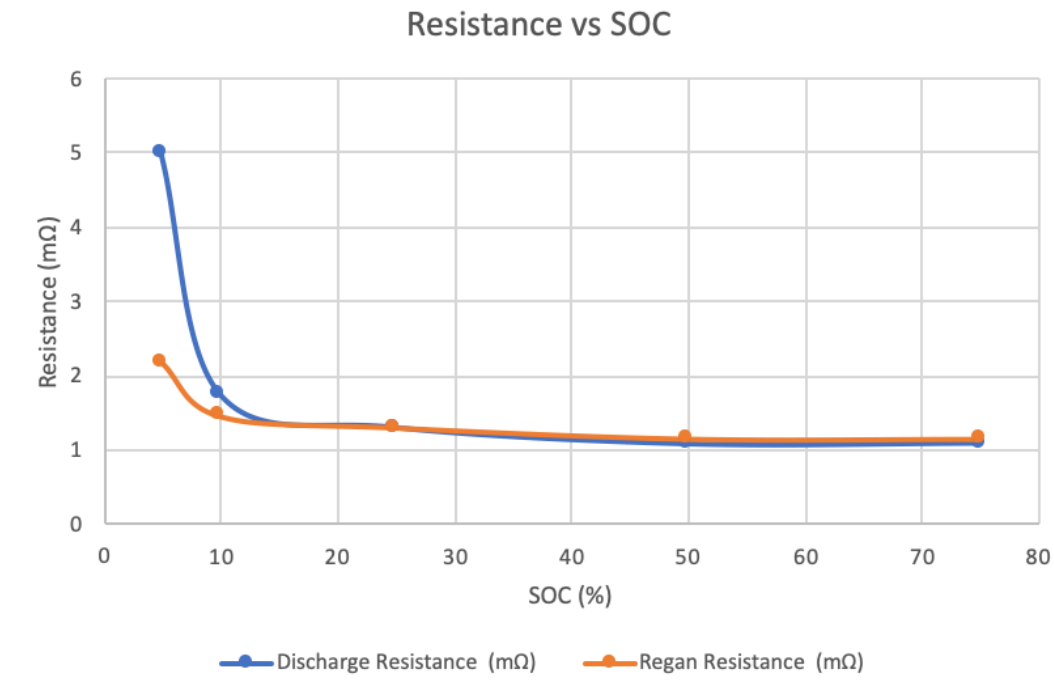

Figure **3-2**: Variation of DCIR with SOC

3.2 Power Density

EVTOL applications require the battery to deliver higher power during the landing and takeoff phases of travel. The specific power that the battery can deliver is strongly dependent on its SOC. For EVTOL applications, the battery must be able to satisfy the power deliver requirements of landing even with a low SOC. Further, an EVTOL battery must have enough reserve power to divert landing in case of an emergency and stay airborne.[10] To analyze the effect of SOC on the specific power of a battery, a step voltage function is created and used as the source voltage in the model. The step voltage function consists of a 10 second 4.15V charge voltage pulse, followed by a period 50 second rest period and then a 2.7V discharge voltage pulse. Current data from the simulation is then used to find the average current values for the time frames of the user defined function. From the charging and discharging data the average charging and discharging powers

can be calculated as:

$$P_{avg} = V_{charging/discharging} * I_{avg} \quad (3.2)$$

Figure 3-3 and Figure 3-4 represent the variation of specific power as a function of the state of charge of the battery. It can be seen that the power available in the cell decreases with decreasing SOC.

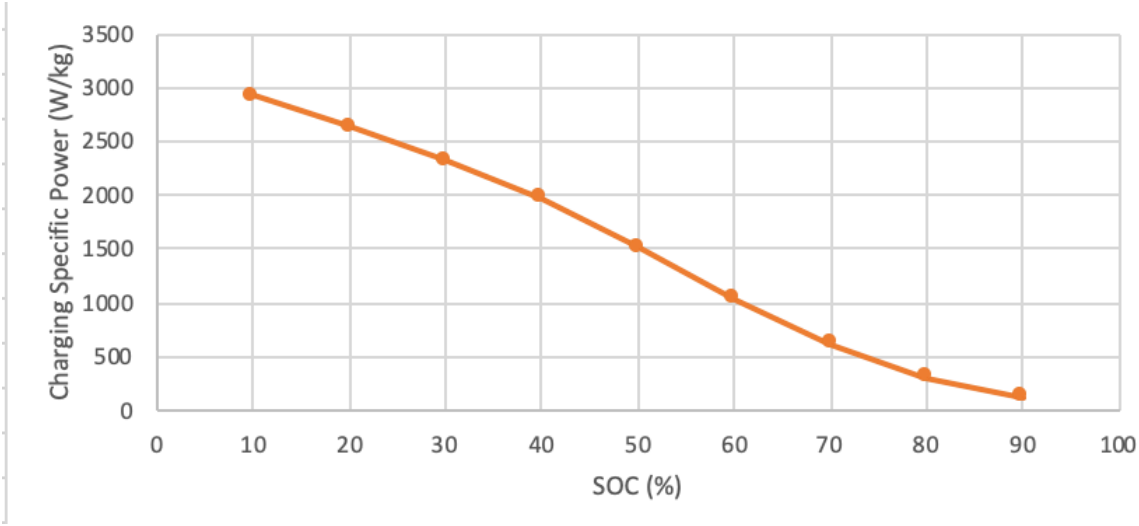

Figure **3-3**: Variation of Charging Specific Power with SOC

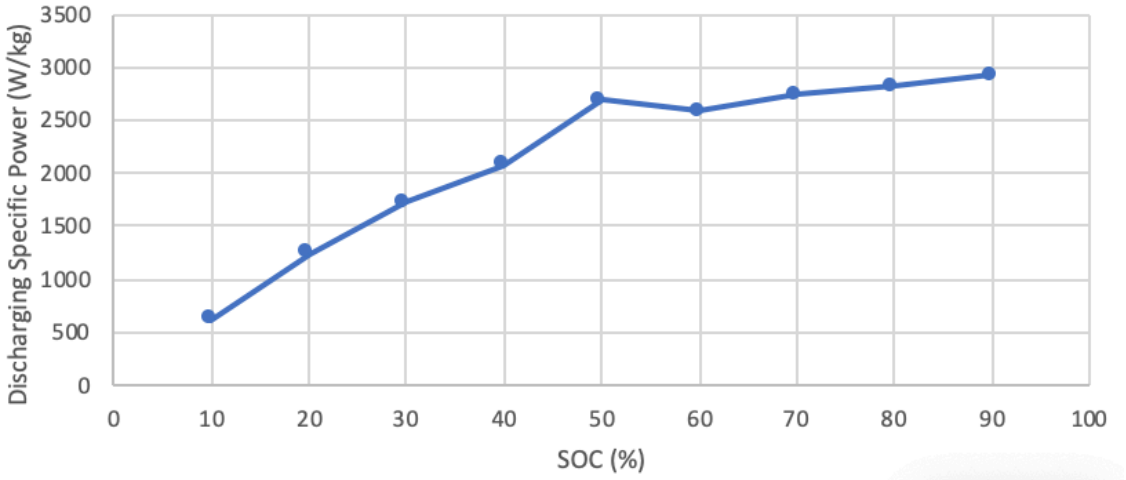

Figure **3-4**: Variation of Discharging Specific Power with SOC

3.3 Key Requirements in EVTOL Applications

Batteries as energy sources of EVTOL have unique requirements. The cruising range of an electric aircraft depends heavily on its specific energy whereas high specific power is a requirement for the landing and takeoff phase of travel.[10] Figure 3-5 illustrates the power and energy requirements for various transportation systems.[16] The dot marked "Exp." represents the current industry standard Li-ion battery that has sufficient specific energy but falls short on the specific power requirements for commercial EVTOLs. A typical EV trip consists of the following phases: takeoff-hover, climb, cruise, descent, and landing hover as depicted in Figure 3-6.[10,17] The specific power required in the takeoff and landing hover can be estimated using equation 3.3 and the specific power required for the climb, cruise and descent can be estimated by equations 3.4, 3.5 and 3.6 respectively[10,17]

$$(SP)_{hover} = \frac{1}{\omega_{battery}} \frac{g}{\eta_h} \left(\frac{\sigma}{2\rho_{air}}\right)^{1/2} \tag{3.3}$$

$$(SP)_{climb} = \frac{1}{\omega_{battery}} \frac{g}{\eta_c} \left(ROC + \frac{V_{climb}}{\frac{L}{D}_{climb}}\right) \tag{3.4}$$

$$(SP)_{cruise} = \frac{1}{\omega_{battery}} \frac{g}{\eta_c} \frac{V_{cruise}}{\frac{L}{D}_{cruise}} \tag{3.5}$$

$$(SP)_{descent} = \frac{1}{\omega_{battery}} \frac{g}{\eta_c} \left(ROD + \frac{V_{descent}}{\frac{L}{D}_{descent}}\right) \tag{3.6}$$

where $\omega_{battery}$ is the weight fraction of the battery, g is the gravitational constant, η_h is the hover efficiency, σ is the disk loading, ρ_{air} is the density of air, η_c is the system efficiency, ROC and ROD are the vertical speed, V is the corresponding true airspeed and $\frac{L}{D}$ is the corresponding lift to drag ratio.

To estimate the specific power requirements for the various phases in an EVTOL the following mission profile is assumed:

1. Takeoff hover lasts for 30 seconds

2. Climb with 50 m/s horizontal speed and 3 m/s vertical speed for 60 seconds
3. Cruise at 70 m/s for 120 seconds
4. Descend with 50 m/s horizontal speed and 3 m/s vertical speed for 60 seconds
5. Landing hover lasts for 30 seconds

An industry standard EVTOL design specifications for battery pack is used as an example for power calculation requirement purposes as shown in Table 3.[10] Using Equations 3.3-3.6, the specific power requirements for different phases of the trip can be calculated as

$(SP)_{hover} = 603.9\, W/kg$

$(SP)_{climb} = 275.4\, W/kg$

$(SP)_{cruise} = 192.2\, W/kg$

$(SP)_{descent} = 44.8\, W/kg$

Given the specific energy of the example battery pack is $200\frac{Wk}{kg}$, a ratio of the specific power to specific energy is calculated for each phase of travel and depicted in Figure 3-7. The power load profile represents that $3\frac{W}{Wh}$ is required during the takeoff/landing, $1.3\frac{W}{Wh}$ during cruise and $0.23\frac{W}{Wh}$ during descent. It can be distinctly seen that the power requirement for the hover phases is about 3 times more than the power requirement during cruise.

Table **3** –EVTOL Design Specification with a 200Wh/kg Battery Pack[10]

Battery Weight Fraction ($\omega_{battery}$)	0.3
Gravitation Constant (g)	9.8 m/s
Hover Efficiency (η_h)	0.64
Disk Loading (σ)	343 N/m^2
Density of Air (ρ_{air})	1.225 kg/m^3
Cruise Efficiency (η_c)	0.85

Length to Drag Ratio during Climb/Descent ($\frac{L}{D_{climb/descent}}$)	12
Length to Drag Ratio during Cruise ($\frac{L}{D_{cruise}}$)	14

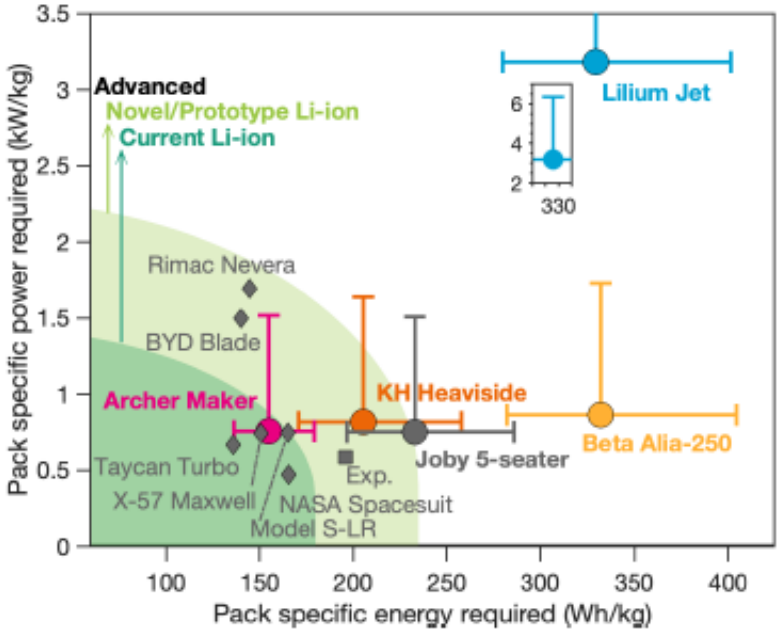

Figure **3-5**: Minimum energy and discharge power requirements for EVTOLs (Sripad, 2021)[16]

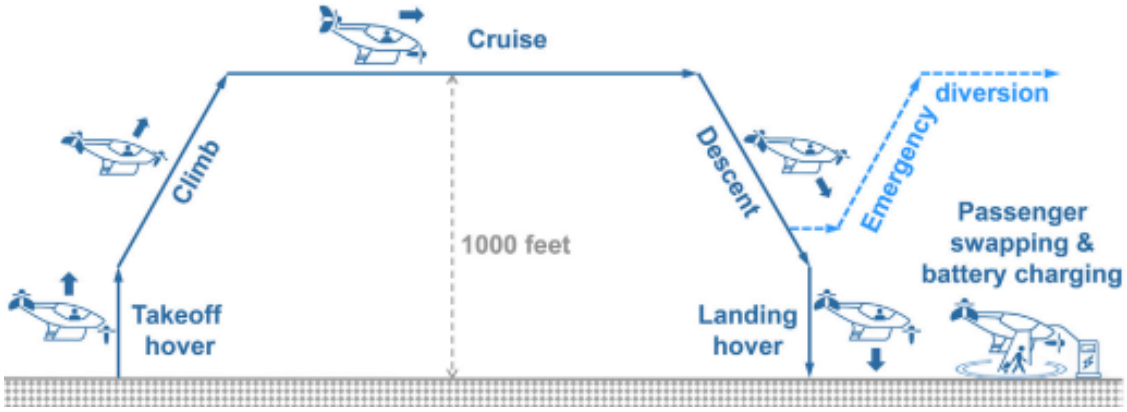

Figure **3-6**: Travel phases in an EVTOL trip (Airbus, 2018)[18]

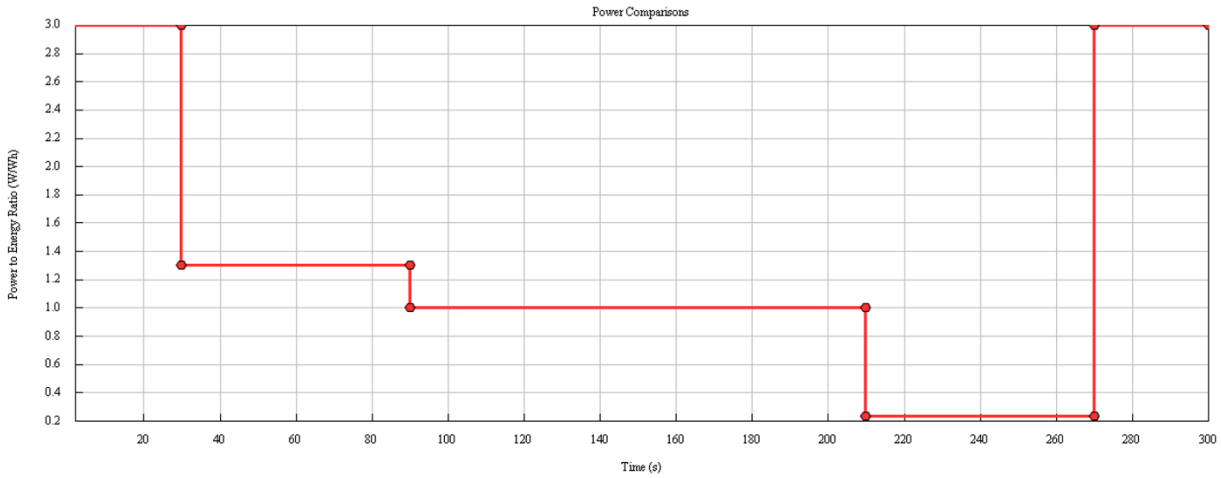

Figure **3-7**: Power Load Profile for a Standard EVTOL Trip

3.4 Thermally Modulated Battery Model

The thermally modulated model is setup in a way that the heating switches could be used to turn-on the Ni foil heating effects as required. Sections 3.4.1 describes the electrical connections that are subjected upon the electrochemical GT-Autolion model for heating and data collection purposes. Section 3.4.2 discusses the energy requirements under the load profile imposed to compare different aircraft ranges. Section 3.4.3 compares the power requirements and the results with and without thermal modulation. Lastly, Section 3.4.4 performs parametric studies to explore the heating effects in further detail.

3.4.1 Model Setup

The electrochemical model created in GT-Autolion is exported into GT-Suite for the addition of electrical connections. As depicted in Figure 3-8, the model uses an internal heat

source in the form of a thin Ni foil whose resistance can be varied in accordance with the supply of heat required. During the landing and takeoff hovers, current passes through the Ni-foil and ohmic heat is generated to heat up the battery from room temperature to 60°C. The ambient temperature control is used to specific an external heat transfer coefficient for forced convection during cruise. For this discussion, we will assume that the ambient temperature is room temperature (20°C) during all phases of the travel. The CCCV serves as a control switch that leads the flow of events within the model. The control switch could be used to turn the heating switches on to heat the battery when required. Further the control switch helps to maintain the forced convection boundary condition which cools the battery down to the ambient temperature.

First, we impose the power load profile on the model as depicted in Figure 3-9. The first and last 30 seconds depicts a takeoff/landing maneuver where the battery is discharging at 3C. Between time 30-90 seconds the EVTOL is in the climb phase with a 1.3C discharge. The cruise phase starts at 90 seconds as the model is incident to a 1C discharge. Lastly, the descent phase lasts between 210-270 seconds as the model is discharging at 0.23C. The model collects temperature, voltage, current and SOC data which is then used to compute the power available during different phases of EVTOL travel.

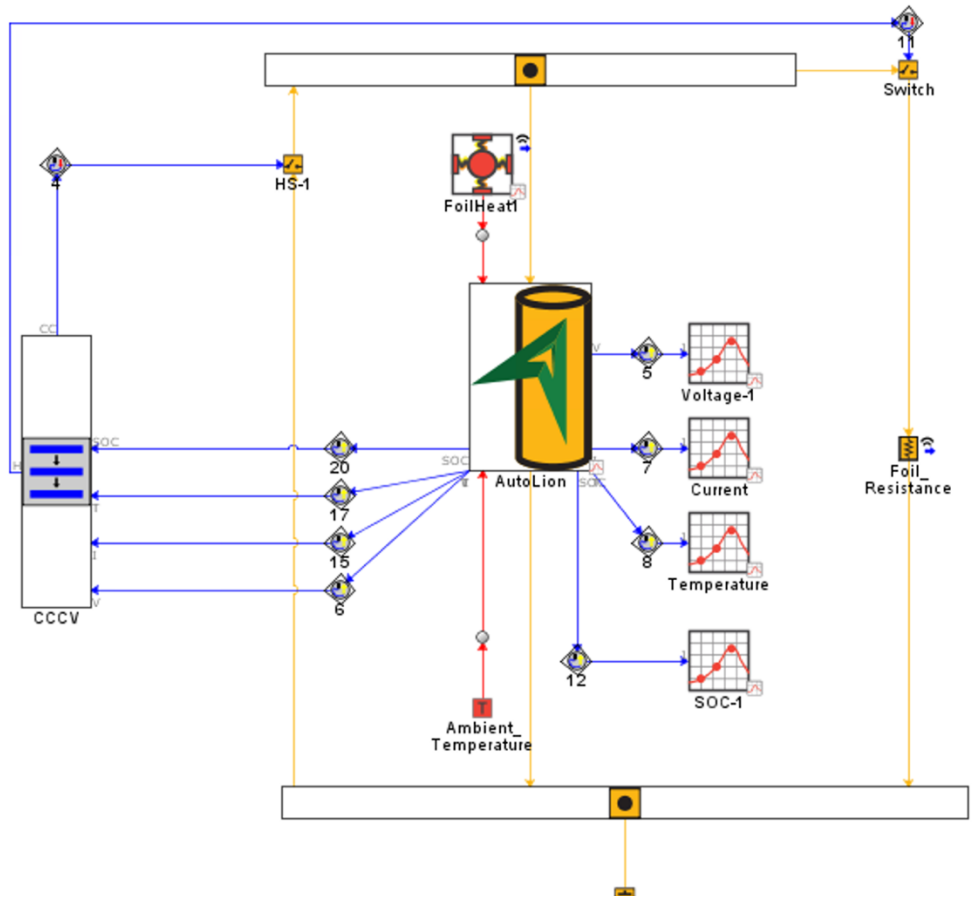

Figure **3-8**: GT-Suite Electrochemical Model for Thermal Modulation

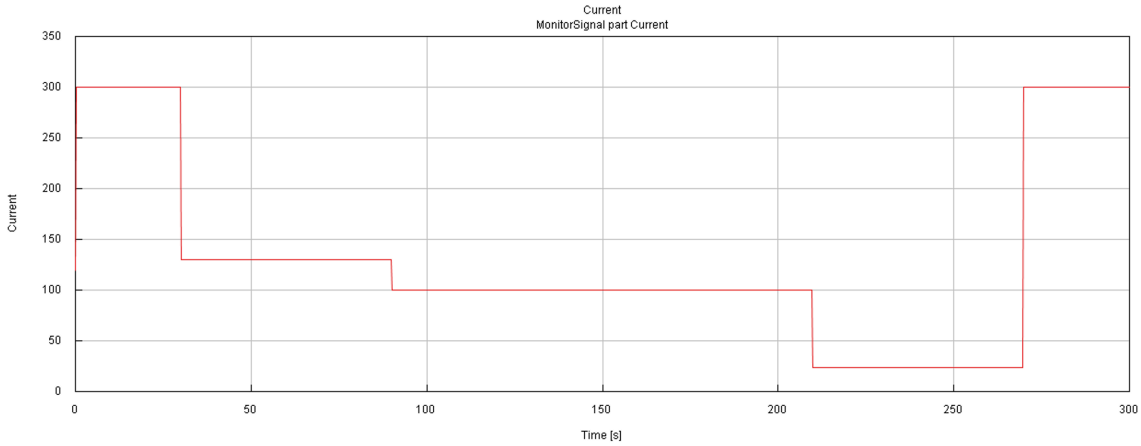

Figure **3-9**: Incident Load Profile on Model

3.4.2 Energy Comparison

The range of travel is dependent on the energy capabilities of the battery. To explore the energy capabilities of the battery, a simulation with 120 seconds, 240 seconds, and 360 cruise times is conducted under the imposed load profile. The ability of the battery to complete the required journey without discharging to the lower cutoff voltage of 2.7V would represent that the battery is capable of satisfying the energy requirement for the travel. Figure 3-10 depicts the results from the simulation. It can be observed that for a cruise period 120, 240 and 360 seconds the battery discharges to 3.76V, 3.72V and 3.68V indicating sufficient available energy in the battery. However, as we learnt in section 3.2, the discharging power of the battery decreases with decreasing SOC. Therefore, before reaching to a conclusion whether the battery completes all requirement for travel at cruise period of 120, 240 and 360 seconds, it is important to explore if the battery has sufficient SOC after the takeoff, climb, cruise and descent phase to provide the required power of 3 $\frac{W}{Wh}$ for the landing maneuver. If sufficient power is not available before the landing phase, thermal modulation can be used to climb over the required power barrier. The power requirements for different cruise timings is explored in more detail in the following section.

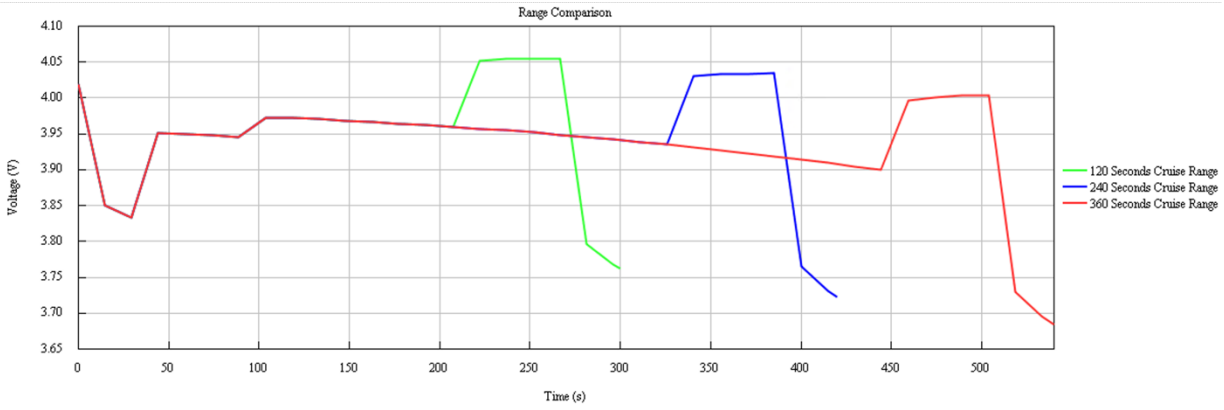

Figure **3-10**: Range Capabilities of the Battery Model

3.4.3 Thermal Modulation Power Comparison

For EVTOL applications it is essential that the battery can provide sufficient power during all phases of travel even at a low SOC. In this section the power capability of the battery is explored. Starting with the 120 seconds cruise time case, the model is subjected to the load power profile and the power results from the simulation is compared with the calculated power requirements as shown in Figure 3-11. The "blue-dotted" curve, representing the output power for the case without thermal modulation, stays above the "red" required power during takeoff, climb, cruise and descent. However, during the landing maneuver, the battery output power falls below the required power barrier. The output power of the battery is below $3\frac{W}{Wh}$ at all times during the landing maneuver and the battery is only able to provide $2.95\frac{W}{Wh}$ before completion of the maneuver.

Heating the battery is an efficient way to decrease the DCIR and provide an easier passage for power to be extracted from the battery. The model is setup to co-simulate the discharge process alongside the heating when the heating switch is turned on as depicted in Figure 3-12. For thermal modulation power comparison purposes, both the power and heating switch is turned on during the takeoff and landing maneuver to heat up the battery while the battery continues to discharge under the 3C load profile. The Ni-foil resistance is chosen in a way such that the battery heats up to 60°C during the 30 seconds landing and takeoff maneuver as shown in Figure 3-13. Forced convection at high air speed causes an exponential decay in temperature during the climb, cruise and descent phase results. The current and voltage data from the simulation is used to calculate the total power of the battery at different phases of travel. For the takeoff and landing maneuver, the power required to self-heat the battery is subtracted from the total power to find the output power of the battery. Figure 3-14 compares the output power of the battery with and without thermal modulation. The output power of the battery increases well

above the required power threshold when heating is turned on during the takeoff and landing maneuver. However, in practical EVTOL applications the battery needs to be pre-heated before the landing maneuver so that the battery is ready to provide the extra power for the landing maneuver. The following sections aims to utilize the concepts of thermal modulation to power the landing maneuver in electric aircrafts.

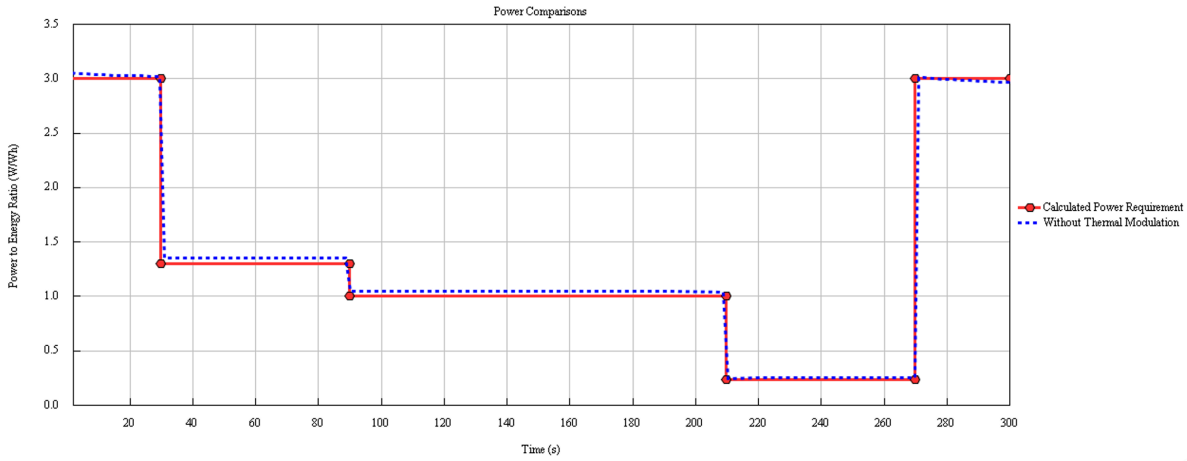

Figure **3-11**: Power Comparison without Thermal Modulation

Event Descriptions	Event Exit Criterion	Next Event No.	Power Switch	CV (1= Current 0 = Voltage)	Heating (1= On 0=Off)	Current Request (A)
Takeoff 3C Discharge	etime >= 30	2	1	1	1	300
Climb 1.4C Discharge	etime >= 60	3	1	1	0	130
Cruise 1C Discharge	etime >= 120	4	1	1	0	100
Descent 0.23C Discharge	etime >= 60	5	1	1	0	23
Landing 3C Discharge	etime >= 30	end	1	1	1	300

Figure **3-12**: Control Switch Depicting Heating alongside Discharge

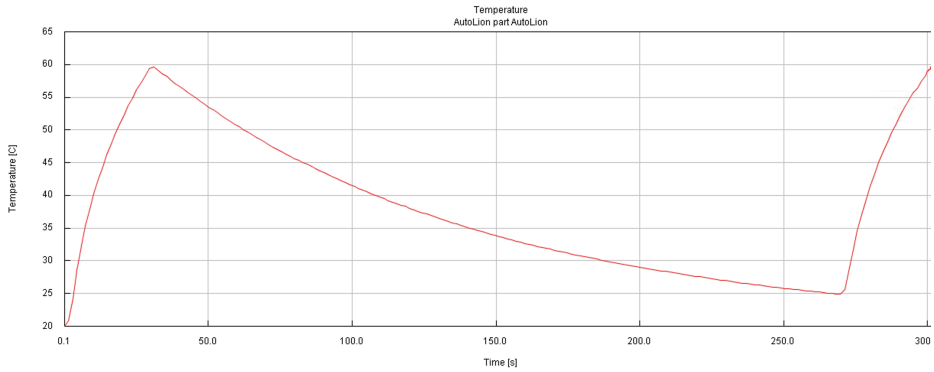

Figure **3-13**: Power Comparison Study Temperature Curve

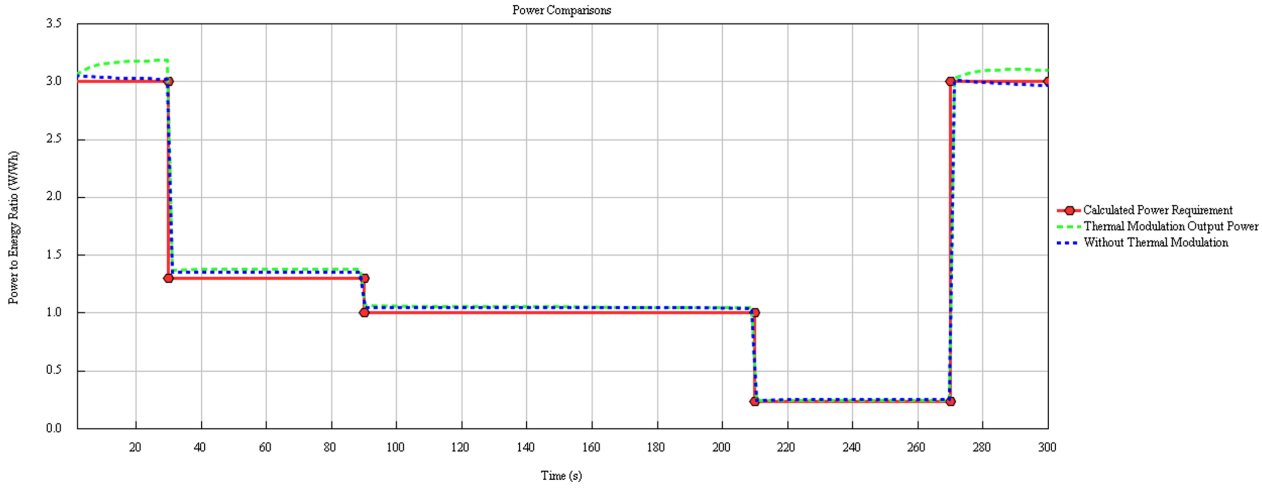

Figure **3-14**: Power Comparison with and without Thermal Modulation

3.4.4 Landing Thermal Modulation

As the battery discharges under the load profile, the SOC of the battery decreases alongside. The battery is at the its minimum SOC before the landing maneuver which also has a high-power requirement. As seen in Section 3.4.3, the battery falls short on providing the power required for the landing maneuver even in the 120 seconds cruise case. This section aims at preheating the battery prior to the landing maneuver to provide the extra on-demand power. The heating switch is turned on during the descent phase at 210 seconds while the EVTOL is preparation to land as seen in Figure 3-15.The temperature increases rapidly from room temperature to 60°C as shown in Figure 3-16. The output power of the thermal modulated simulation is plotted alongside the results of the same case without thermal modulation in Figure 3-17. Similar simulations are conducted for a cruise period of 240 seconds and 360 seconds and the power comparisons are plotted in Figure 3-18 and Figure 3-19 respectively. It can be seen that the battery operating at elevated temperatures during the landing phase is well able to

successfully complete the landing maneuver in all cruise cases which would not have been possible otherwise.

Event Descriptions	Event Exit Criterion	Next Event No.	Power Switch	CV (1= Current 0 = Voltage)	Heating (1= On 0=Off)	Current Request (A)
Takeoff 3C Discharge	etime >= 30	2	1	1	0	300
Climb 1.4C Discharge	etime >= 60	3	1	1	0	130
Cruise 1C Discharge	etime >= 120	4	1	1	0	100
Descent 0.23C Discharge	etime >= 60	5	1	1	1	23
Landing 3C Discharge	etime >= 30	end	1	1	0	300

Figure **3-15**: 120 Seconds Cruise Landing Control Switch

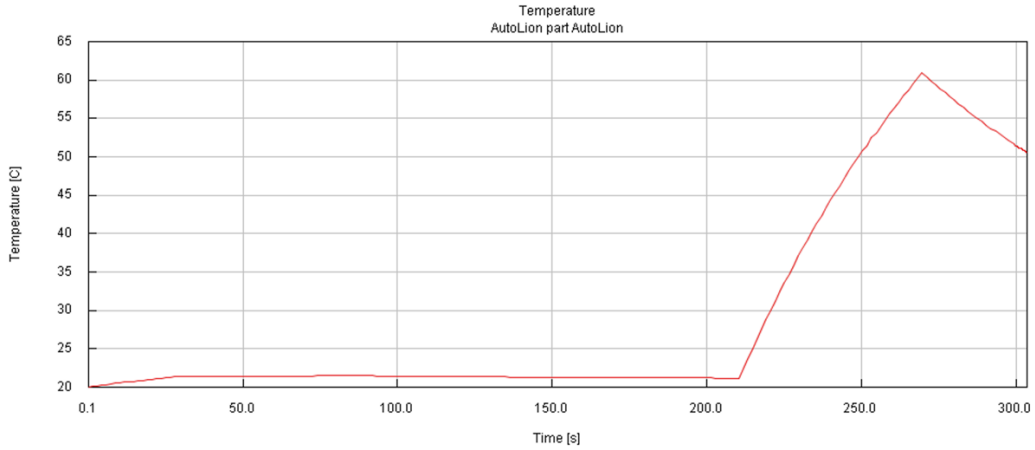

Figure **3-16**: 120 Seconds Cruise Landing Study Temperature Curve

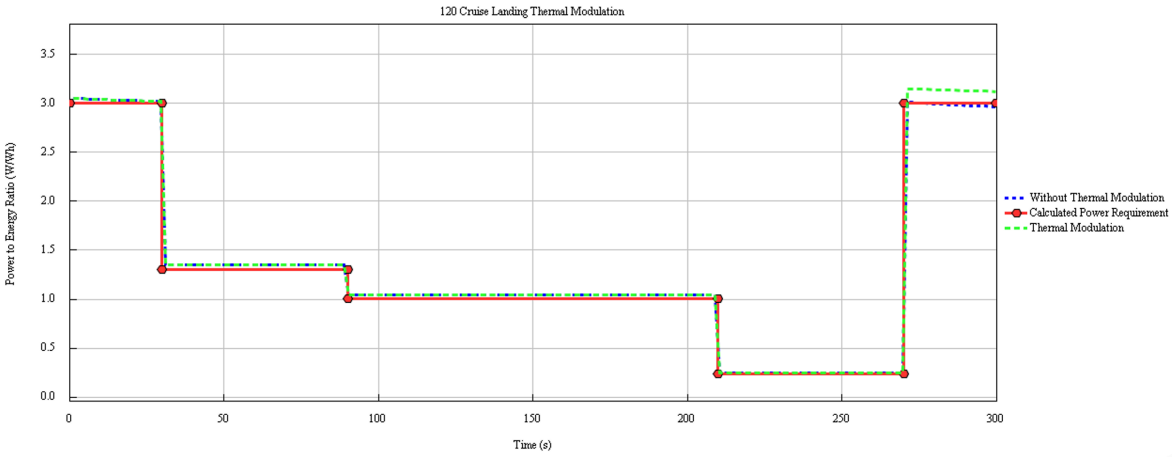

Figure **3-17**: 120 Seconds Cruise Landing Study Power Curves

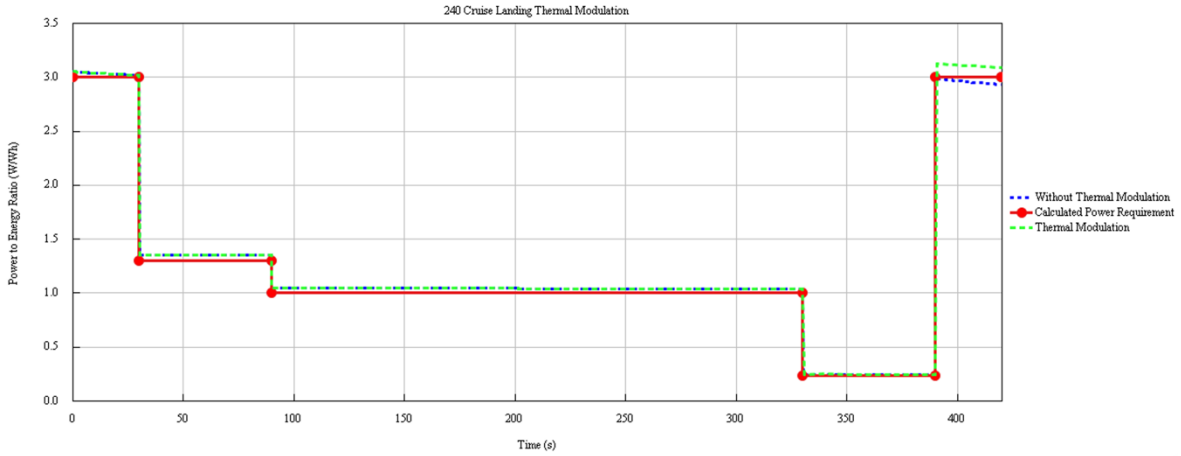

Figure **3-18**: 240 Seconds Cruise Landing Study Power Curves

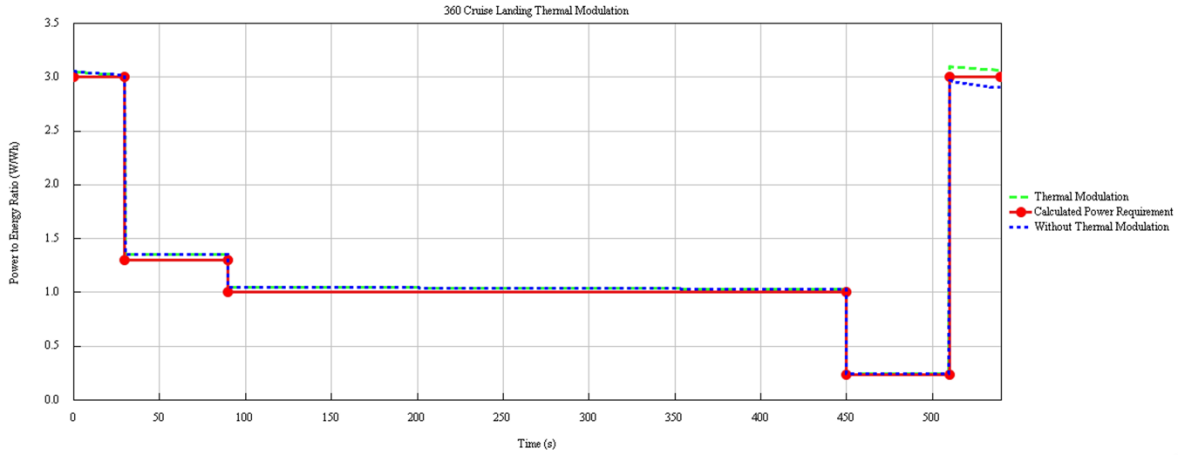

Figure **3-19**: 360 Seconds Cruise Landing Study Power Curves

3.4.4 Slow Heating

This parametric study is conducted for a cruise period of 250 seconds and involves varying the resistance of the Ni-foil such that the battery heats up gradually over an extended time period. Initially the heating switch is turned on for the takeoff and climb phases. The heating

switch is turned off once the EVTOL is in cruise and the temperature decreases exponentially due to the forced convection at high air speeds as seen in Figure 3-20. Once the cruise phase is completed, the heating switch is turned on again for the descent and landing phases to cater to the high-power requirement of landing. Figure 3-21 can be used to visualize the output power performance of the thermally modulated battery and the one without thermal modulation for this specific scenario. The battery model without thermal modulation would fail during landing as the battery wouldn't provide enough power to complete the landing maneuver which can be seen by the "blue-dotted" lines falling below the "red" required power curve. The "green-dotted" curve, representing the output power for the thermally modulated case, stays above the power requirements during all phases of travel. Hence, the thermally modulated battery would be able to satisfy the power requirements for the journey alongside the energy requirements as investigated in Section 3.4.2.

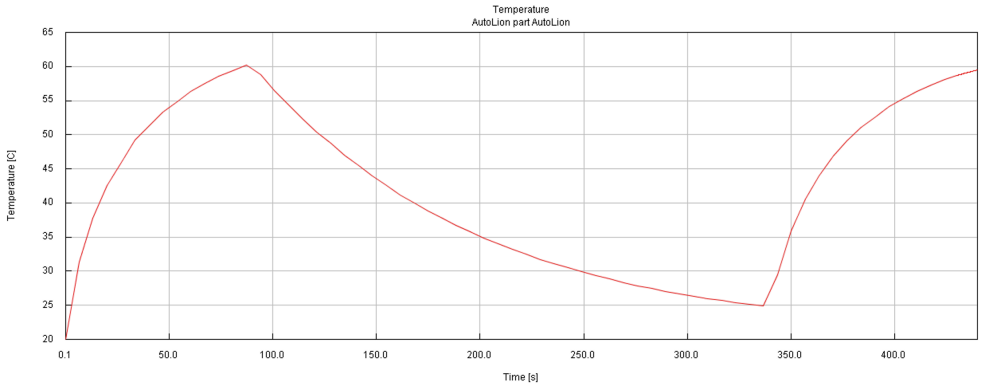

Figure **3-20**: Slow Heating Temperature Curve

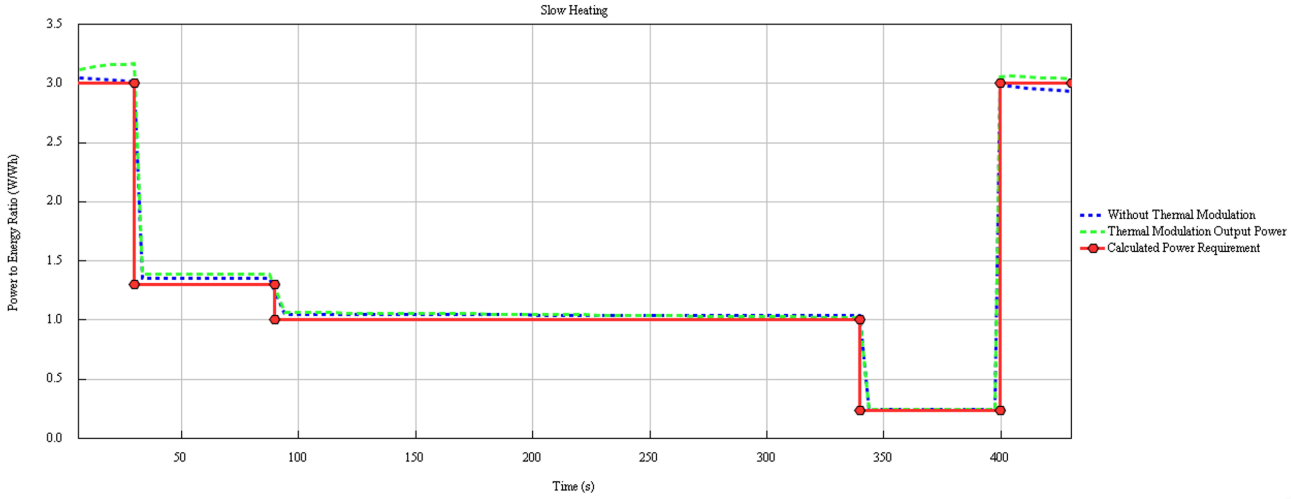

Figure **3-21**: Slow Heating Power Comparisons

Chapter 4

Conclusions and Future Work

4.1 Conclusions

Technological advancements have enabled us to find ways to decrease our dependency on fossil fuels and accelerate our transition towards sustainable sources of energy. Battery technology has been in the forefront of this transition. There lies a need to scavenge for disruptive technologies that can revolutionize the future. The use of electric vertical and takeoff landing aircrafts for travel falls into this futuristic category. Modern day Li-ion batteries have sufficient energy density to enable an EVTOL complete short distance travel. However, they fall short on the power density requirements. This thesis proposes the use of thermal modulation to increase the power density of Li-ion batteries for electric aircraft applications. The power requirements during takeoff and landing are significantly more than the power required during other phases of travel.

Operating the battery at elevated temperature during the takeoff and landing phases provides an efficient way to extract power on-demand from the battery without increasing the battery size. Chapter 1 introduced the principle and working of a Li-ion battery. In this study, NMC is used as the cathode material and Graphite is used as the anode. During discharge the Li ions de-intercalate from the stored anode sites and move to the cathode through the separator via diffusion. To model this phenomenon and conduct simulations a pseudo-2D model (P2S) approach proposed by Newman and Doyle is used via GT-Autolion.

Chapter 2 described the fundamental equations that the commercial software GT-Autolion uses to conduct coupled electrochemical and thermal studies of battery systems. An electrochemical model of an 100Ah battery was created on GT-Autolion, following the design specifications obtained from our lab. The model was calibrated and experimentally validated at different temperatures to ensure the model predictions were consistent with experimental data at the operating temperature ranges.

Chapter 3 conducted studies on how different battery parameters change with varying temperature and SOC's. It was concluded that increasing the battery temperature decreases the DCIR and provides an easier passage for power to be extracted from the battery. It was also noticed that the power density decreases with decreasing SOC and therefore the landing maneuver in EVTOL applications was a point of further study. EVTOL applications have different power requirements during the landing, climb, cruise, decent and takeoff phase. The power requirement for each of these phases was calculated. The Autolion model was imported into GT-Suite and electrical connections were added to create a model capable of provide a heating mechanism to the battery via a Ni-foil. The power load profile was incident on the model and results were obtained for various case scenarios.

The energy requirement was first compared for different cruise timings. It was observed that the battery had sufficient energy to complete travel for cruise periods of 120, 240 and 360 seconds.

The power requirement fulfillment was then subjected to analysis in the 120, 240- and 360-seconds cruise cases. It was observed that the battery did not have sufficient power to complete the landing maneuver. Thermal modulation was used to raise the battery temperature to 60°C prior to landing to provide additional power and successfully complete the landing maneuver. A parametric study was conducted for a cruise period of 250 seconds and the Ni-foil resistance was varied for a more gradual heat supply. The results clearly demonstrated that thermal modulation could be used to overcome the calculated power barrier for EVTOL maneuvers.

4.2 Future Work

Further analysis on the safety of the battery system must be conducted before the cell can be used in commercial applications. Thermal runaway incidents in Li-ion battery can be lethal and result in releases of significant amount of energy. The self-heating step during thermal modulation results in an increase in the battery current. Since the heat generated in the battery is proportional to square of the current, the heat generated is this step is also very large.[10] The battery management system must be well adapted to deal with these sudden changes in current and must disconnect the battery before a catastrophic failure. Further, the battery pack must be designed in a way that prevents cell-to-cell propagation in the case a thermal runaway event was to occur.[10] In case of an emergency landing or deviation, the battery must also have enough reserve power to successfully complete additional maneuvers.[10]

References

[1] GREENCARS. How many electric vehicles sold in 2021? 2021; Available from https://www.greencars.com/post/how-many-electric-vehicles-sold-in 2021#:~:text=Worldwide%2C%20electric%20vehicle%20sales%20are,first%20half%20of%20the%20year

[2] Wong, Kai Wai, and Wan Ki Chow. "Principle for the Working of the Lithium-Ion Battery." *Journal of Modern Physics*, vol. 11, no. 11, 2020, pp. 1743–1750., https://doi.org/10.4236/jmp.2020.1111107.

[3] Su, Boman, Xinyou Ke, and Chris Yuan. "Electrochemical Modeling of Calendar Capacity Loss of Nickel-Manganese-Cobalt (NMC)-Graphite Lithium-Ion Batteries." arXiv preprint arXiv:2103.02166 (2021)

[4] Newman, J., Tiedemann, W. (1975) Porous-electrode theory with battery applications. *AIChE Journal*, 21: 25-41.

[5] Zhou, Jiaping, et al. "A Review of Lithium-Ion Batteries Electrochemical Models for Electric Vehicles." *E3S Web of Conferences*, vol. 185, 2020, p. 04001., https://doi.org/10.1051/e3sconf/202018504001.

[6] Haran, B.S., Popov, B.N., White, R.E. (1998) Determination of the hydrogen diffusion coefficient in metal hydrides by impedance spectroscopy. *Journal of Power Sources*, 75: 56-63.

[7] Huang, L., Yao, C. (2016) Working Condition RealTime Monitoring Model of Lithium-Ion Batteries Based on Distributed Parameter System and Single Particle Model. *Chinese Journal of Chemical Physics*, 29: 623-628.

[8] Luo, W., Lyu, C., Wang, L. (2013) A new extension of physics-based single particle model for higher charge–discharge rates. *Journal of Power Sources*, 241: 295-310.

[9] Goto, I., Ohkuma, H., Hongo, H. (2016) Feasibility Study of Modified Single-Particle Model for Composite Cathode at High-Rate Discharge. *Electrochemistry*, 84: 432-437.

[10] Yang, Xiao-Guang, et al. "Challenges and Key Requirements of Batteries for Electric Vertical Takeoff and Landing Aircraft." *Joule*, vol. 5, no. 7, 2021, pp. 1644–1659., https://doi.org/10.1016/j.joule.2021.05.001.

[11] Li, Dongjiang & Danilov, Dmitri & Bergveld, H. & Eichel, Rüdiger-A & Notten, Peter. (2019). CHAPTER 9: Understanding battery aging mechanisms. 10.1039/9781788016124-00220.

[12] Liu, Teng, et al. “Effect of Thermal Environments on Fast Charging Li-Ion Batteries.” *Journal of Power Sources*, vol. 511, 2021, p. 230466., https://doi.org/10.1016/j.jpowsour.2021.230466.

[13] W. B. Gu and C. Y. Wang, Thermal-electrochemical modeling of battery systems. *Journal of the Electrochemical Society*, 147(8), 2910-2922 (2000).

[14] Ji, Yan (2013), Low Temperature Operation of L-ion battery for Hybrid and Electric Vehicles. Pennsylvania State University.

[15] Yang, Xiao-Guang, et al. “Thermally Modulated Lithium Iron Phosphate Batteries for Mass-Market Electric Vehicles.” *Nature Energy*, vol. 6, no. 2, 2021, pp. 176–185., https://doi.org/10.1038/s41560-020-00757-7.

[16] Sripad, S., & Viswanathan, V. (2021). The promise of energy-efficient battery-powered urban aircraft. Proceedings of the National Academy of Sciences, 118(45). https://doi.org/10.1073/pnas.2111164118

[17] Kasliwal, A., Furbush, N. J., Gawron, J. H., McBride, J. R., Wallington, T. J., De Kleine, R. D., Kim, H. C., et al. (2019). Role of flying cars in sustainable mobility. Nat. Commun. 10, 1555.

[18] Airbus. (2018). Urban air mobility iconography. https://acubed.airbus.com/blog/airbus-utm/ urban-air-mobility-iconography/.

[19] CHAPTER 9: Understanding battery aging mechanisms - Scientific Figure on ResearchGate. Available from: https://www.researchgate.net/figure/representation-of-the-shape-and-components-of-various-Li-ion-battery-configurations_fig3_331753941 [accessed 18 Feb, 2022]

[20] Kalupson, J., Luo, G., and Shaffer, C., "AutoLion™: A Thermally Coupled Simulation Tool for Automotive Li-Ion Batteries," SAE Technical Paper 2013-01-1522, 2013, https://doi.org/10.4271/2013-01-1522.

[21] P. Lima, Samsung SDI 94 Ah battery cell full specifications, 2021. https://pushevs.com/2018/04/05/samsung-sdi-94-ah-battery-cell-full-specifications/.

[22] Y. Ji, Y. Zhang, C.-Y. Wang, Li-ion cell operation at low temperatures, J. Electrochem. Soc. J. Electrochem. Soc. 160 (2013) 636–649, https://doi.org/10.1149/2.047304jes.